Accuracy Assessment of Li-ion Batteries Internal Resistance Model Through CFD Simulations, Experimental Measurements And Uncertainties

Elie Solai, Héloïse Beaugendre, Ulrich Bieder, Pietro Marco Congedo

ACCURACY ASSESSMENT OF LI-ION BATTERIES INTERNAL RESISTANCE MODEL THROUGH CFD SIMULATIONS, EXPERIMENTAL MEASUREMENTS AND UNCERTAINTIES

E. Solai*, H. Beaugendre, U. Bieder, P.M. Congedo
*Author for correspondence
Inria, Univ. Bordeaux, CNRS, Bordeaux INP, Institut de Mathématiques de Bordeaux,
Bordeaux, 33000, France
E-mail: elie.solai@inria.fr

ABSTRACT

Internal resistance is a critical parameter of the thermal behavior of Li-ion battery cells. This paper proposes an innovative way to deal with the uncertainties related to this physical parameter using experimental data and numerical simulation. First, a CFD model is validated against an experimental configuration representing the behavior of heated Li-ion battery cells under constant discharging current conditions. Secondly, an Uncertainty Quantification based methodology is proposed to represent the internal resistance and its inherent uncertainties. Thanks to an accurate and fast to compute surrogate model, the impact of those uncertainties on the temperature evolution of Li-ion cells is quantified. Finally, a Bayesian inference of the internal resistance model parameters using experimental measurements is performed, permitting to reduce the prediction uncertainty by almost 95% for some temperatures of interest.

INTRODUCTION

The widespread use of electric vehicles forces manufacturers to build high-performance cars and provide the ability of fast charging for consumers. High-intensity currents demanded by these capabilities can generate intense heat loads on the battery pack of the vehicle [2]. Operating the car and battery pack under high temperatures can seriously damage the Li-ion batteries and reduce the lifespan of the whole system [10]. Then, industrial efforts are focused on Battery Thermal Management System (BTMS) to keep the batteries in a safe range of temperature during charging and discharging sequences. Understanding and predicting the thermal behavior of Li-ion cells is then crucial to improve these systems.

The heat generated by Li-ion cells is, for the most part, caused by the Joule effect, coming from the electric current going through the Li-ion cells and its inherent internal resistance. The complex chemical structure of Li-ion cells and electrochemical reactions occurring within it are responsible for obstruction in electrons transfer and, thus, internal resistance. The internal resistance depends then on many uncertain parameters such as temperature, state-of-charge of the cell and their combined effect. Developing an accurate model to represent its behavior is a challenging topic [5; 8].

In the present work, a novel methodology to improve the numerical solver's predictive character using Uncertainty Quantification methods and experimental measurement is presented. The code TrioCFD is used to compute the thermal behavior of heated Li-ion cells under discharging conditions. This CFD tool is validated for the first time in literature against an experimental configuration of battery cells. Then, the uncertainties of the internal resistance of Li-ion cells are modeled and propagated through the CFD solver to assess their impact on the temperature evolution of the Li-ion cells under discharging conditions. Finally, a Bayesian inference of the internal resistance model is performed using experimental measurements, to reduce the numerical prediction uncertainty.

NOMENCLATURE

$\mathbf{u}$	[m/sec]	Velocity field in fluid domain
T	[K]	Temperature field
p	[Pa]	Pressure field in fluid domain
t	[sec]	Time
$R(T)$	[mΩ]	Internal resistance model
I	[A]	Electrical current intensity
C	[-]	Unit of discharge rate
q_g	[W/m^2]	Heat source term in solid equation
C_p	[J/(kg/K)]	Specific heat
d, h	[mm]	Diameter and height of the Li-ion cells
$\overline{R} = [R_0, ..., R_3]$	[mΩ]	Resistance vector, surrogate model input
$\overline{T}$	[K]	Temperatures vector, surrogate model output
$\overline{T}^{exp}$	[K]	Experimental measured temperatures vector

Special characters

ν	[m^2/s]	Kinematic viscosity
ρ	[kg/ m^3]	Density
λ	[W/(mK)]	Thermal conductivity
$\alpha = \lambda/\rho C_p$	[m^2/s]	Thermal diffusivity
$\Omega, \Omega_f, \Omega_s$	[-]	Computational domains
N_{LHS}	[-]	Number of simulations in the design of experiment
N_{exp}	[-]	Number of available experimental measurements
$\mathcal{M}$	[-]	Surrogate model function
$\mathbb{P}$	[-]	Probability

Subscripts

$_{f,\ s,\ i}$	Fluid domain, Solid domain, Fluid/solid interface

EXPERIMENTAL AND CFD TEST CASE

Experimental Test Case

The experiment reproduced in this study is taken from [3]. The set-up consists in two parallel rows of four Li-ion cells each (see Fig. 1). The Li-ion cells used in the experiment are cylindrical 26650 cells, with LiFePO4 chemical composition. A battery pack, composed of two rows of cells, is between enclosure walls made of plexiglass. Each cell present a diameter of $d = 25.85$ [mm] and height of $h = 62.5$ [mm], with a given spacing between cells illustrated in Fig. 1. A constant discharging electric current is applied to the Li-ion cells during the whole experiment time. According to the discharge rate of 1.5 [C], the current across the entire battery pack is set to $I = 6.9$ [A]. This discharge current is applied to the cells from the beginning of the experiment, at time $t_0 = 0$ [sec] until the final time $t_f = 1600$ [sec].

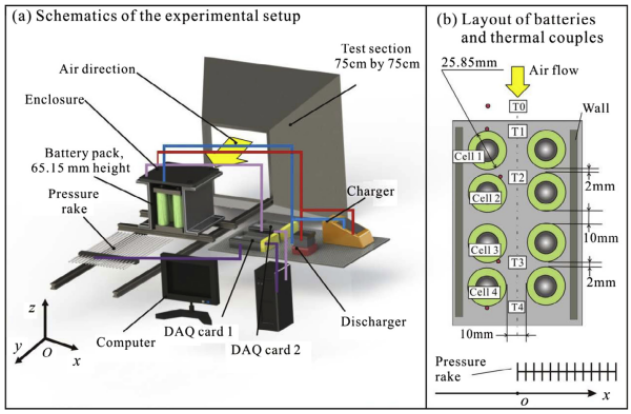

(a) (b)

Figure 1. Experimental set up. Figure courtesy of [3]

The purpose of the experiment is to monitor the temperature evolution of the heated Li-ion cells measured at key locations of each cell surface. The probes positions are represented by the black cross on Fig. 1-b. In this experiment, the temperature evolution of the cells is studied under various airflow conditions. The case of forced convection with a non zero inlet velocity in the fluid domain, is treated, for numeric validation purposes. Then, the uncertainty quantification study on the internal resistance model is performed in the case of pure heating of the cells, with no air inlet velocity. One scope of the present work is to consider the data coming from the experiment with the uncertainties related to the measured quantities of interest and with the inherent uncertainties of physical parameters involved in Li-ion cell heating.

Governing Equations and CFD Model

To represent numerically the experimental case, a two-dimensional simulation of the transient conjugate heat transfer is performed. The computational domain Ω is divided in two sub-domains: the fluid domain and solid domain. Because of the symmetry of the experimental set-up the full domain Ω represents only half of the physical set up, namely, one plexiglass wall and only one row composed of four cells, like shown in Fig. 2.

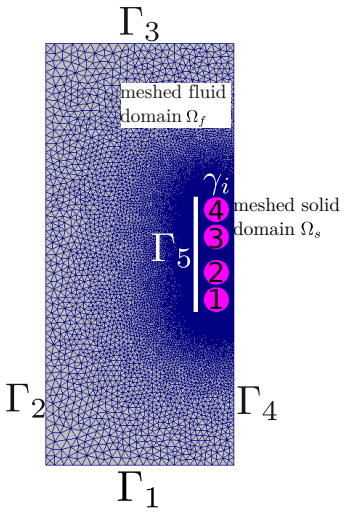

Figure 2. Mesh, computational domains and boundary labels for the CFD simulation.

In the fluid domain Ω_f, the Navier-Stokes equations are solved along with the energy equation. The set of equations in the fluid domain reads:

$$\begin{cases} \nabla \cdot \mathbf{u} &= 0 \\ \frac{\partial \mathbf{u}}{\partial t} + \mathbf{u} \cdot \nabla \mathbf{u} &= \nabla \cdot (\nu_f \nabla \mathbf{u}) - \frac{1}{\rho_f} \nabla p \\ \frac{\partial T}{\partial t} + \mathbf{u} \nabla T &= \nabla \cdot (\alpha_f \nabla T) \end{cases} \tag{1}$$

The solid domain Ω_s represents the four heated cells. The heat equation is solved in this part of the domain. The heat equation in Ω_s reads:

$$\frac{\partial T}{\partial t} = \nabla \cdot (\alpha_s \nabla T) + \frac{q_g}{\rho_s C_{p,s}} \tag{2}$$

At the interface γ_i between the two domains Ω_f and Ω_s, the coupling conditions related to conjugate heat transfer are applied: temperature and heat flux continuity. Let's denote $T_{f,i}$ and $T_{s,i}$ the temperature on the interface in the fluid and solid domains respectively. Similarly, $\Phi_{f,i}$ and $\Phi_{s,i}$ are the heat flux coming out of the fluid and solid domain respectively. For any instant t of the simulated time, the temperature and heat flux continuity are expressed by:

$$T_{f,i} = T_{s,i} \qquad \Phi_{f,i} = -\Phi_{s,i} \tag{3}$$

The source term in the solid domain Ω_s represents the heat generated by the Joule effect, due to the discharge current I applied to the cells, and their internal resistance R. The details

about the source term expression are explained further in the article. However, to complete the equations' description, the expression of the source term in eq. 2 is given by:

$$q_g = R(T) \cdot I^2 \tag{4}$$

q_g being a volumic source term, it is applied to each mesh element of the solid domain. Then the resistance depends on the temperature evaluated in each element of the discretized solid domain. The numerical tool used to solve the governing equations is TrioCFD [1], which is a numerical tool developed at CEA for heat transfer and fluid problems oriented towards nuclear applications. Note that TrioCFD is applied here for the first time in litterature to the simulation of battery cells. The conditions on the different boundaries indicated in Fig. 2 are the following ones: Γ_1 imposed temperature and velocity, Γ_2 symmetry and adiabatic for thermal equations, Γ_3 free outlet, Γ_4 symmetry, Γ_5 wall condition, γ_i coupling conditions (fluid/solid interface). TrioCFD provides the predicted temperature evolution at the probes locations showed in Fig. 1.

Evaluation of the Numerical Schemes

The purpose of this section is to make sure that the numerical schemes used to solve flow and thermal equations in TrioCFD are consistent with an already validated numerical tool on this kind of heat transfer problems. A code to code comparison is performed, between TrioCFD and the code used in [3], FLUENT. The test case is set up with the following conditions: an air flow of $\mathbf{u} = 1$ [m/s] is imposed at the inlet boundary. The heat from solid domain is provided by a constant source term $q_g = 6.666 \cdot 10^3$ [W/m^2] in eq. 2. For this case of forced convection with inlet velocity, a Low-Re $k-\varepsilon$ turbulence model [4] is added to eq. 1. The 2D mesh contains $1.7 \cdot 10^4$ nodes. The temperature evolution is computed at the probes positions, specified in Fig. 1. As the two numerical codes are set with the same heating conditions, it's assumed that if TrioCFD reproduces the same temperature evolution as FLUENT, the flow and heat equations are numerically solved with good consistency.

Fig. 3 shows the temperature evolution at the probes position computed by TrioCFD and FLUENT. Both codes give similar temperature prediction. Thus, from these results, confidence is gained about the numerical settings chosen for the case and the ability of TrioCFD to compute conjugate heat transfer in a case of heated Li-ion cells.

CFD Simulation for the Case of No Inlet Velocity: Resulting Temperature Field

Here a simulation in the case of pure heating is presented, i.e. with air velocity set to $\mathbf{u} = 0$ [m/s] at inlet boundary. A Dirichlet boundary conditions is applied to the temperature of the inlet boundary ($T_{inlet} = 295.2$ [K]). The same value is used for the initial condition in the whole domain. An adiabatic wall condition is applied to symmetry boundaries for the temperature.

This representation of the temperature field in Fig. 4 highlights the process of transient conjugate heat transfer. The heat

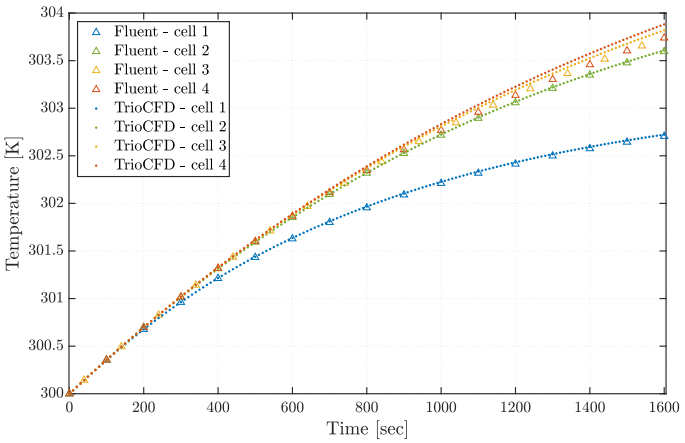

Figure 3. Numerical temperature prediction from FLUENT and TrioCFD at the probes positions, for each battery cell.

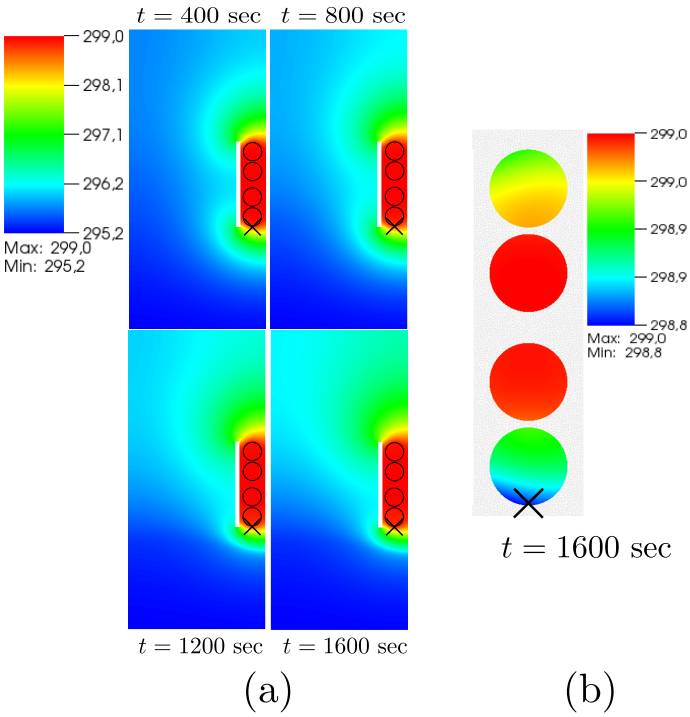

Figure 4. (a) Contour plot of the temperature field evolution in solid and fluid domains. (b) Focus on the temperature field in the solid domain at $t = 1600$ [sec]. data is measured.

is generated in the solid domain Ω_s with the volumic heat source q_g from eq. 4. Then the heat is spread through the solid domain according to the conduction equation in eq. 2. The fluid in Ω_f surrounding the solid domain is retrieving the heat generated through the coupling conditions in eq. 3. The air temperature and resulting flow is computed with eq. 1. Also, increased heat loads for the cells 2 and 3 can be expected, because of the cell arrangement and the wall on the side. This configuration, even

if simple, can show the issues of cooling in real battery packs where several Li-ion cells are set up close to each other.

MODELING UNCERTAINTIES IN INTERNAL RESISTANCE MODEL

Now that the description and ability of the CFD model to solve the problem of heated cells has been shown, the focus is set on studying the uncertainties related to the internal resistance model.

A Priori Choice of the Internal Resistance Model

To consider uncertainties in the internal resistance values, it is first required to choose an a priori structure for the model to represent this function. From many references studying properties of Li-ion batteries, it is a good guess to assume that the internal resistance is dependent on the temperature only, in a cubic polynomial form [8]. The objective here is then to build a direct relationship between the resistance of the cell and its temperature, following some physical constraints, *i.e.* $T \mapsto R(T)$. Specifically, the built model $R(T)$ is imposed to be strictly decreasing within the temperature range of the experiment following several works [5; 7].

A Bezier parametrization is chosen to model the resistance, requiring the definition of some control points. Note that expected monotonic behavior of the resistance can be naturally imposed with a suitable choice of the control points. Within the range of relevant temperatures with respect to usual Li-ion cells problems, four values of temperature are selected, equally spaced, as input values. Then, for these selected temperature values, four corresponding values of internal resistance are taken. This process outcomes in four temperature-resistance control points. Then, the model is built using a Bezier curve parametrization. An illustration of the Bezier parametrization in modelling the resistance $R(T)$ is given in Fig. 5 with five curves and their associated control points (corresponding to the same colour), within the range of temperature of the experiment (represented by the vertical red dotted lines). Note that the mathematical behavior of each model is controlled through the variability of the control points.

Uncertainty Characterization in the Internal Resistance Model

Using the Bezier parametrization, the uncertainties of the internal resistance can be represented, modelling the distribution of the control points variability. In practice, a random variable R_i is introduced, giving the resistance value at the temperature abscissa $T_i, i \in [0,3]$ of each control point. The uncertainties of each resistance (for a given temperature abscissa T_i) are assumed to follow a given uniform distribution. For this reason, a physically sound interval of variation is considered, from which the resistance values can be obtained. For one sampled set of resistance values $\overline{R}^{(i)} = [R_0, ..., R_3]$ the corresponding Bezier polynomial model $R^{(i)}(T)$ is built and ready to be implemented in the CFD code through the source term q_g from eq. 2.

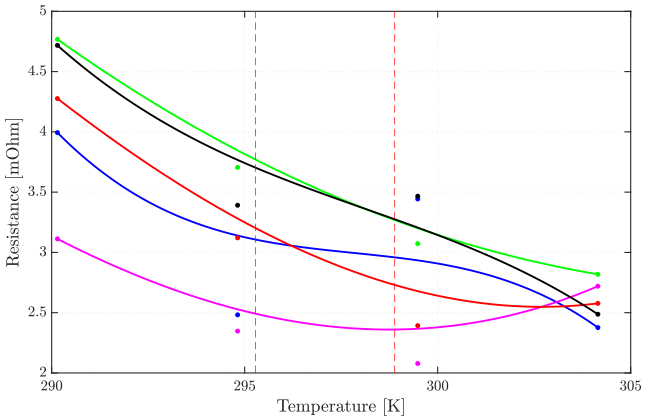

Figure 5. Five samples of the Bezier control points and corresponding $R(T)$ curves (matched by colors). The red dotted lines represent the temperature range of the experiment. The four abscissa of the control points are: $T_0 = 290$ [K]; $T_1 = 294.8$ [K]; $T_2 = 299.5$ [K]; $T_3 = 304.1$ [K]

CALIBRATION OF THE RESISTANCE MODEL PARAMETERS USING EXPERIMENTAL DATA AND SURROGATE MODEL

Surrogate Model and Uncertainty Propagation

Using the process detailed in the previous section the uncertainties inherent to the internal resistance model can be modeled. The objective of this whole study is to assess the impact of these uncertainties on the temperature response of the heated Li-ion battery cells. A so-called Uncertainty propagation problem consists in propagating the input uncertainties through the numerical solver (the CFD solver in this case) to compute a statistical distribution of a specific quantity of interest. The target here is the computation of some statistics of the temperature evolution on the Li-ion cells surface.

A simple approach to compute these statistics is the classical Monte Carlo method. It is very effective but expensive, though. In fact, it requires the evaluation of many samples to converge properly, which correspond in this case to many CFD expensive evaluations. Many values of the temperature response are required, each corresponding to an evaluation of the computational model with an internal resistance model $R^{(i)}(T)$ as input. This turns to be prohibitive with the present CFD model which presents a high computational cost.

The approach followed here is then to build a surrogate model of the quantity of interest as a function of the input parameters, which can be used instead of evaluating the CFD model. Practically, let's define for the surrogate model the input as a vector of four sampled values of resistance $\overline{R} = [R_0, ..., R_3]$. The output is represented by a vector $\overline{T}$ of k temperature values $\tilde{T}_k$, at different times of the experiment t_k, on the location specified in Fig. 4, such that $\tilde{T}_k = \tilde{T}(t_k)$. The surrogate model just defined is described in eq. 5:

$$\mathcal{M} : \overline{R} = [R_0, ..., R_3] \mapsto \overline{T} = [\tilde{T}_1, ..., \tilde{T}_k] \tag{5}$$

The construction of this function is performed using the Gaussian process regression theory [9]. The idea is to build an interpolation function from a set of construction points constituting a so-called Design of Experiment (DOE). In this case, Latin Hypercube Sampling (LHS) technique was used to sample N_{LHS} models for the internal resistance $R^{(i)}(T), i \in [1, N_{LHS}]$. Then, a CFD simulation is performed for each input $\overline{R}^{(i)}$, providing the output vector of temperature values $\overline{T}^{(i)}$. Fig. 6 illustrates the evaluation of temperatures by the surrogate model for an input $\overline{R}^{(i)}$ versus the (exact) one evaluated with CFD, showing an excellent accuracy of the surrogate model. Fig. 7 illustrates the surrogate model's envelope on the whole stochastic space, which overlaps with the experimental measurements (and the corresponding error bars).

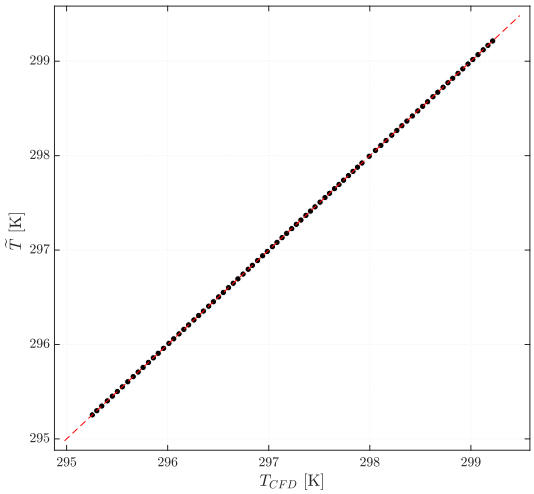

Figure 6. Comparison of surrogate model evaluations of temperature $\tilde{T}$ with the CFD model for a given input $\overline{R}^{(i)}$. The red line represents the first bisector curve.

Bayesian Calibration of the Resistance Model Parameters

In this section, the attention is set on the calibration of the input parameters of the resistance model. The first approach is to perform a deterministic calibration by minimizing the L2 error between the temperature predictions from the CFD model and the experimental measurements. The L2 error, for a CFD run with a given input model $R(T)$ is defined by the sum of discrepancies between the temperature evaluated by the CFD model and temperature measured experimentally at each time t_j where a data is available.

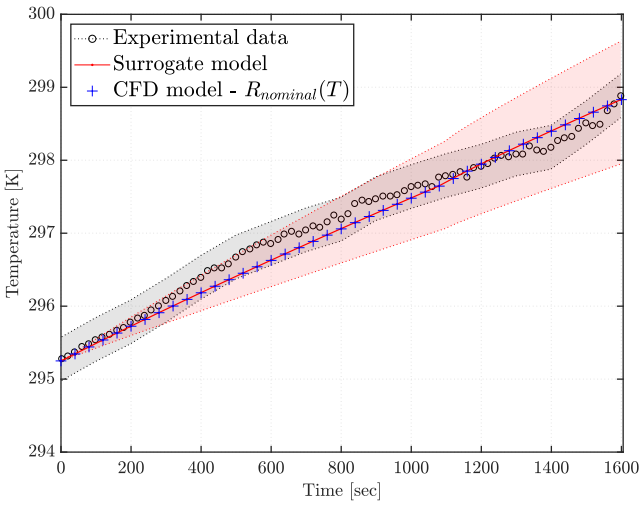

Figure 7. Surrogate model response with its variation envelope due to input uncertainties (red). Comparison with experimental data and its measurement error envelope (black). CFD model response with nominal input model $R_{nominal}(T)$ (blue).

$$Error_{\mathbb{L}_2}(R(T)) = \sum_{j=1}^{N_{exp}} \left(T^{CFD}(R(T), t_j) - T_j^{exp} \right)^2 \tag{6}$$

From the many CFD simulations in the plan of experiment, an other surrogate model f is built, mapping the values of resistance $\overline{R}$ with the corresponding L2 error. Then an optimization problem is run to get the values of input $\overline{R}$ which minimizes the function f. This outcomes in an optimized vector called $\overline{R}_{L2}$ defining a $R_{L2}(T)$ model which gives the closest CFD response from experimental measurements, in Fig. 8 (green). The resulting CFD computation using this input resistance model can be seen in Fig. 9 (green).

The second approach is to consider a Bayesian calibration of the parameters [6]. The objective is to compute the distribution of the input parameters $\overline{R} = [R_0, ..., R_3]$ which leads to the model response the closest to the experimental data in a Bayesian sense. Specifically, the goal is to compute the distribution of the input parameters $\overline{R}$, conditioned to the experimental data $\overline{T}^{exp}$. Following Bayes theorem, the following relation between the posterior distribution, the likelihood and the prior distribution reads:

$$\mathbb{P}[\overline{R}|\overline{T}^{exp}] \propto \mathbb{P}[\overline{T}^{exp}|\overline{R}] \cdot \pi(\overline{R}) \tag{7}$$

where $\mathbb{P}[\overline{R}|\overline{T}^{exp}]$ is the posterior distribution, $\mathbb{P}[\overline{T}^{exp}|\overline{R}]$ the likelihood and $\pi(\overline{R})$ the prior distribution. The objective of the Bayesian calibration is to compute the posterior distribution.

In this case, first, a prior distribution to the input parameters is defined, *i.e.* $\overline{R} \sim \pi(\overline{R})$. There is no a priori information on the

input values, except an acceptable range of variation, and then a non-informative prior (uniform distribution) is chosen. The posterior distribution is obtained using a Markov Chain Monte Carlo algorithm.

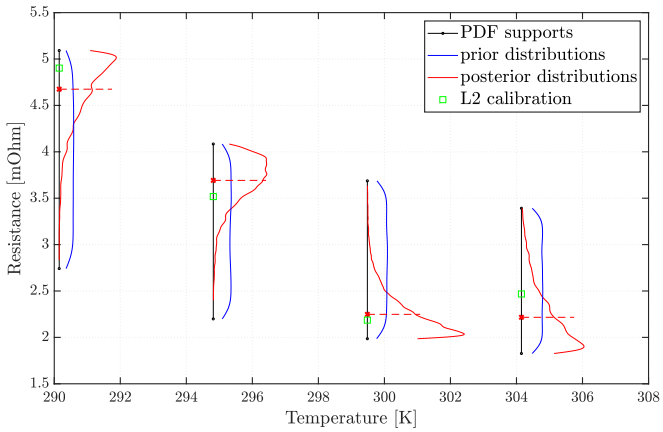

Figure 8. Prior (blue) distributions and posterior (red) distributions of input parameters after Bayesian calibration. In green, resulting values of resistance after deterministic calibration.

The uncertainty propagation of the input prior distributions (Fig. 8 - blue) leads to a considerable variation on the numerical prediction of temperature (Fig. 9 - blue), which envelops experimental data systematically. Considering the posterior distributions (Fig. 8 - red), the uncertainty on the input parameters has been reduced by 73%, 76%, 75%, 47% for the parameters R_0, R_1, R_2, R_3 respectively. Furthermore, the Bayesian inference allows gaining knowledge on the numerical model response. Fig. 9, shows the temperature distributions (red) predicted by the surrogate model, resulting from the propagation of posterior input distributions from Fig. 8. The posterior predicted distributions are more narrow than the priors. For instance, the uncertainty for the predicted temperature at $t = 1517$ [sec] (Fig. 9) is reduced by 98% using the posterior distributions of input parameters. Then, by including the knowledge from the experimental data, the uncertainty on the model response has been reduced, and the quality of the numerical model prediction can be assessed from a more relevant perspective.

CONCLUSION

In the present work, an Uncertainty-based internal resistance model was formulated to solve a conjugate heat transfer problem of heated Li-ion batteries. A forward propagation of uncertainties and Bayesian calibration of the input parameters were performed, thanks to an accurate surrogate model. This outcomes in a more relevant assessment of the numerical prediction quality regarding the system's physical behaviour. Overall, uncertainty on the predicted temperatures has been reduced by 95%, and uncertainty on some input parameters has been reduced by 75%.

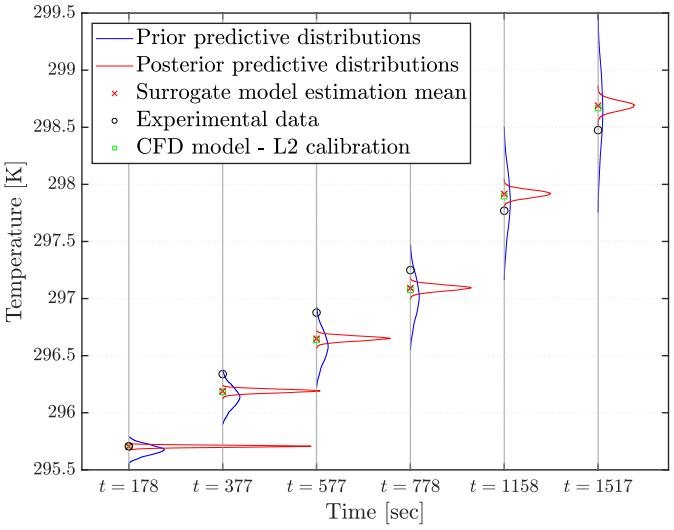

Figure 9. Prior (blue) and posterior (red) predicted distributions of the quantities of interest. In green, result of the CFD model with the $R_{L2}(T)$ input model.

REFERENCES

[1] TrioCFD: http://www-trio-u.cea.fr.

[2] Kim S.-J. Lamp P. Lux S.F. Maglia F. Paschos O. Stiaszny B Andre, D. Future generations of cathode materials: An automotive industry perspective (review). *Journal of Materials Chemistry A*, 2015.

[3] Fan He, Xuesong Li, and Lin Ma. Combined experimental and numerical study of thermal management of battery module consisting of multiple Li-ion cells. *International Journal of Heat and Mass Transfer*, 72:622–629, May 2014.

[4] W.P Jones and B.E Launder. The prediction of laminarization with a two-equation model of turbulence. *International Journal of Heat and Mass Transfer*, 15(2):301–314, February 1972.

[5] G. Karimi and X. Li. Thermal management of lithium-ion batteries for electric vehicles. *International Journal of Energy Research*, 37(1):13–24, January 2013.

[6] Marc C. Kennedy and Anthony OHagan. Bayesian calibration of computer models. *Journal of the Royal Statistical Society: Series B (Statistical Methodology)*, 63(3):425–464, 2001.

[7] Yong Li, Lifang Wang, Chenglin Liao, Wu Lingfei, Li Junfeng, and Guo Yanjie. Effects of temperature on dynamic characteristics of li-ion batteries in electric vehicle applications. In *2014 IEEE Conference and Expo Transportation Electrification Asia-Pacific (ITEC Asia-Pacific)*, pages 1–6, Beijing, China, August 2014. IEEE.

[8] Chanwoo Park and Arun K. Jaura. Dynamic Thermal Model of Li-Ion Battery for Predictive Behavior in Hybrid and Fuel Cell Vehicles. pages 2003–01–2286, June 2003.

[9] C.E. Rasmussen. *Gaussian Process for Machine Learning*. The MIT Press, 2006. Massachusets Institute of Technology.

[10] Noboru Sato. Thermal behavior analysis of lithium-ion batteries for electric and hybrid vehicles. *Journal of Power Sources*, page 8, 2001.